Design study of the divertor Thomson scattering system for JT-60SA

Shin Kajita[1)], Takaki Hatae[2)], Kiyoshi Itami[2)], Noriyasu Ohno[3)], Tomohide Nakano[2)]

[1)]*EcoTopia Science Institute, Nagoya University, Furo-cho, Chikusa, Nagoya 464-8603, Japan*

[2)]*Japan Atomic Energy Agency, Ibaraki 311-0193, Japan*

[3)]*Graduate School of Engineering, Nagoya University, Nagoya 464-8603, Japan*

(Received: 28 October 2009 / Accepted: 15 January 2010)

Feasibility study of the divertor Thomson scattering measurement system for JT-60SA is carried out. A case study of different optical configurations reveals that both laser transmission optics and collection optical system are to be embedded in the lower narrow port plug. From the perspective of the laser induced damage threshold, the size and the material for the laser transmission mirror are assessed. Moreover, the performance of the detection system with using polychromator is investigated by use of numerical method, and the transmission wavelength ranges of optical filters are optimized. It is shown that four detector channels are at least necessary for the polychromator, and the measurement accuracy becomes the highest when the detector channel is six.

Keywords: Thomson scattering measurement, JT-60SA, divertor plasma

1 Introduction

The aim of JT-60SA (JT-60 Super Advanced) is to contribute to the early realization of fusion energy by its exploitation in support and supplement of the ITER program, by addressing key physics issues for ITER and DEMO. In JT-60SA, heat flux to the divertor plate may exceed 10 MWm^{-2}, which is close to the limit for divertor material; control of the divertor plasmas is particularly important for long-pulse discharges. It is expected to produce a dense and cold plasma in the upstream of the divertor target and to reduce the heat flux to the target. The measurements of the electron density, n_e, and temperature, T_e, in the divertor plasmas are crucial for that purpose.

In cold recombining plasmas, it has been reported that current-voltage characteristics of electrostatic probe was distorted, and, consequently, the measurement overestimated T_e [1,2]. Spectroscopic method using line intensity ratios of helium atom has been used for the measurement of n_e and T_e; however, the radiation transport would alter the intensity ratio, particularly when the cold plasma was adjacent to hot ionizing plasmas [3,4]. Thomson scattering measurement is reliable diagnostics to measure n_e and T_e, and it has also been applied to cold plasmas in DIII-D [5] and a linear divertor simulator [6]. It is expected that direct measurements of n_e and T_e in the divertor region by the Thomson scattering measurement help to control the divertor plasmas in JT-60SA. Note that the required measurement ranges for the electron temperature and density are 1 – 100 eV, and $> 10^{20}$ m^{-3}, respectively.

In this paper, feasibility study of the divertor Thomson scattering system in the geometry of JT-60SA is carried out. In Sec. 2, design studies of collection optical system and laser transmission optics are provided. In Sec. 3, a numerically optimized filter design for the polychromator, i.e. the detection system, is presented.

author's e-mail: kajita.shin@nagoya-u.jp

2 Optical System

2.1 Case study for the measurement configuration

For a laser Thomson scattering measurement system, a laser beam and a collection optical system are installed in the plasma device. For an initial assessment, a case study of three different optical configurations is conducted. It is noted that only an upper and lower vertical ports will be available for the measurement system. Figure 1(a), (b), and (c) show the cross sectional illustrations of JT-60SA. Figure 1(a) and (b) show the configuration of case (i) and (ii), respectively, in which the laser is injected from the lower port and collection optical system is also embedded in the lower port plug. In case (i), the laser is horizontally injected, and the scattering signal is collected from a lower position. In contrast, in case (ii), scattering signal is detected from horizontal direction, and the laser is injected from a lower position. Figure 1(c) shows the configuration of case (iii), in which laser is injected from the upper port and the collection optical system is embedded in the lower port. Here, the important points to be taken care of are the feasibility of the collection optical system, the laser transmission mirror, and beam dump for the laser beam, which is inevitable to decrease the stray light.

Table 1 shows the several important parameters that indicate the performance of the system for the three cases: the distance between the first mirror and the measurement point, scattering angle θ_s, and mirror radius for the measurement assuming that necessary solid angle is 0.01 steradian. For each case, two or three measurement points are chosen. In case (i), it is seen that mirror radius, which corresponds to necessary radius of the entrance pupil, be-

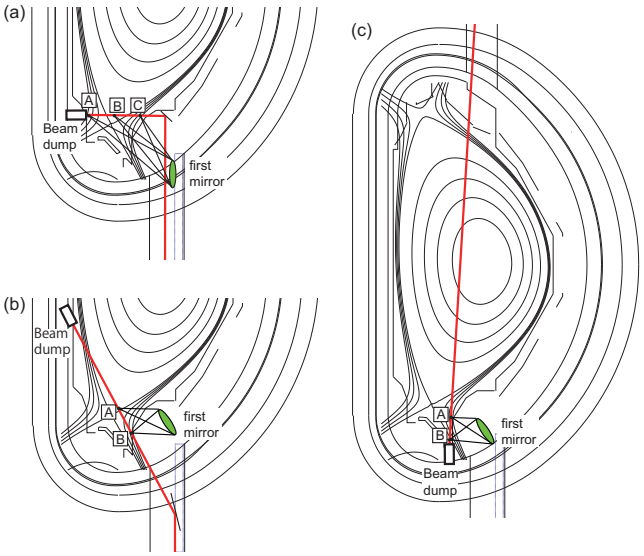

Fig. 1 Illustration of the divertor Thomson scattering system in JT-60SA. (a) and (b) show the cases when the laser is injected from the lower port, and (c) shows the case when the laser is injected from the upper port.

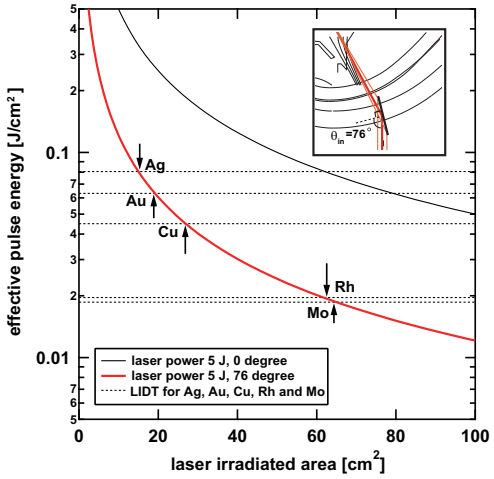

Fig. 2 Effective laser pulse energy is plotted against the laser irradiated area. The laser pulse energy and incident angle for the mirror were assumed to be 5 J and 76 degree, respectively. In addition, the case for 0 degree is also shown as reference. Calculated multi-pulse LIDT [7] is plotted for different mirror materials as dotted lines.

comes larger because the distance between the mirror and measurement point is longer than the other cases. For point A in case (i), the diameter of the mirror should be approximately 20 cm, and it may be hard to equip such a large mirror in the lower port. It is noted that width of the divertor cassette is 3 cm, and the plasma is observed through a 3 cm-slit by removing a cassette. Thus, the available solid angle would be smaller than 0.01 steradian in actual configuration.

If the laser beam was injected from the upper port, like in case (iii), the beam dump should be embedded in the divertor plate, as shown in Fig. 1(c). Since the laser beam is focused at the measurement point, and the distance between the beam dump and the measurement point is so close, the laser power density at the beam dump would exceed the limit for the vaporization of material in case (iii). For the laser transmission mirror, metallic mirror will be used for the last one, which is embedded in the vacuum vessel, because it is durable for the radiation rather than coating mirrors. However, since they are vulnerable to the damages by the particles from plasmas [7], they should be located away from the plasma. Thus, case (ii) is better than case (i) from the point of the laser transmission mirror. Conclusively, the case (iii) is eliminated because of the beam dump, and case (ii) is better than case (i) in the light of the solid angle and laser transmission mirror. Thus, comparing the three different designs, the best design seems to be case (ii). In this study, as a preliminary assessment for possible divertor Thomson scattering system, case (ii) is used for required calculations.

Table 1 The distance between the measurement point and first mirror, scattering angle, and necessary mirror radius for the cases 1–3.

		distance [m]	scattering angle [degree]	mirror radius [cm]
case 1	A	1.65	145	9.3
	B	1.32	135	7.4
	C	1.05	119	5.9
case 2	A	0.79	135	4.5
	B	0.58	103	3.3
case 3	A	0.59	71	3.3
	B	0.58	106	3.3

2.2 Laser transmission optics

Concerning the laser transmission mirror, the size is determined from the perspective of laser induced damage threshold (LIDT). Figure 2 shows the laser pulse energy as a function of the laser irradiated area assuming that the laser pulse energy and pulse width are 5 J and 30 ns, respectively, which are typical parameters of the laser used for Thomson scattering [8]. Since the wave incident on the final mirror will have *s*-polarization, the reflectivity will increase with the angle θ_{in}, which is the angle between the normal vector of the mirror surface and the wave vector, as shown in the inset of Fig. 2. Consequently, the LIDT will also increase with θ_{in}; it increases by a factor of $1/\cos(\theta_{in})$ from that for the case of normal direction [9]. In Fig. 2, effective laser pulse energy, which includes the effect of the angle dependence by effectively decreasing the laser pulse

energy by a factor of $1/\cos(\theta_{in})$, is plotted for the cases of 0 and 76 degree. Since the incident angle θ_{in} is 76 degree for case (ii), the LIDT increases approximately by a factor of four compared with the case of normal laser irradiation.

Dotted lines represent the calculated LIDTs [7] for Ag, Au, Cu, Rh, and Mo by considering multi-pulse effect. Even though Rh and Mo have lower sputtering yield, they have much lower LIDT than those for Ag, Au, and Cu. Moreover, Cu is much cheaper than Ag and Au, the mirror can be made of bulk material for Cu, though coating technique should be applied for Au in particular. Corrosion may easily take place for Ag mirror and deteriorate the reflectivity. Thus, it seems that Cu is one of the best choices for the first mirror material. From Fig. 2, the cross points between the intersection of the curve and dotted lines deduce the necessary mirror sizes. For Cu and Ag mirrors, for example, necessary areas are 27 cm^2, and 15 cm^2, respectively. Here, another point to be considered is the size of the slender lower port plug, which is approximately 3 cm × 25 cm. Assuming that the laser beam shape is circular, and the diameter is 2.5 cm, laser irradiated area is 20.3 cm^2 by considering the incident angle of 76 degree. Thus, the laser pulse energy exceeds the LIDT for Cu, though it is lower than the LIDT for Ag. Therefore, when choosing Cu for the mirror material, laser beam shape should be elliptical rather than circular. Given that the shape of the laser beam is elliptical and the major and minor diameters are 2.5 cm and 5.0 cm, respectively, the laser irradiated area becomes 41 cm^2, and the laser pulse energy is lower than the LIDT for Cu.

Since it is necessary to focus the laser beam on the measurement points, and the distance between the mirror and the measurement points is approximately 1.5 m, the laser mirror should be a parabolic mirror with a focal length of ~1.5 m. Furthermore, a laser beam dump is inevitable on the opposed wall. The size becomes comparable to the assumed laser beam size of 2.5 × 5.0 cm. We have to keep in mind that a fairly larger beam dump than the actual laser beam size is required to sufficiently decrease the stray light.

3 polychromator

Concerning the spectroscopic system, polychromator with optical filters and avalanche photodiodes (APDs) are planned to be used. The same type of polychromator has been widely used for the laser Thomson scattering systems using a Nd:YAG laser [10]. In the core Thomson scattering system, we have to consider hydrogen Balmer spectra at 656 nm [11]. In contrast, for the divertor Thomson scattering system, there is concern that impurity lines, such as the emission from carbon ions, may overlap the Thomson scattering signal around the laser wavelength of 1064 nm. Figure 3(a) shows the spectral density function of the Thomson scattering signal [12] at several different temperatures for θ_s = 120 degree. It is seen that the Thomson spectrum is mainly in the wavelength range over 1000 nm when the covered temperature is lower than 100 eV. Figure 3(b) shows the relative intensities of C I, He I, He II, and H I obtained from NIST (National Institute of Standards and Technology) database [13]. Although the relative intensities were also checked for ionized carbon species, i.e. C II, C III, C IV, and C V, there were no strong lines in the wavelength range of 900–1100 nm. Strong emissions can be observed at less than 970 nm, ~1070 nm for C I, and 1080 nm for helium. Detailed analysis using Monte Carlo transport cord and collisional radiative model for estimating the emission intensity would be necessary to confirm the effect of those emissions. However, fortunately, it is found that the overlaps of the Thomson scattering signal with the impurity lines may not be significant in the wavelength range of 970-1064 nm.

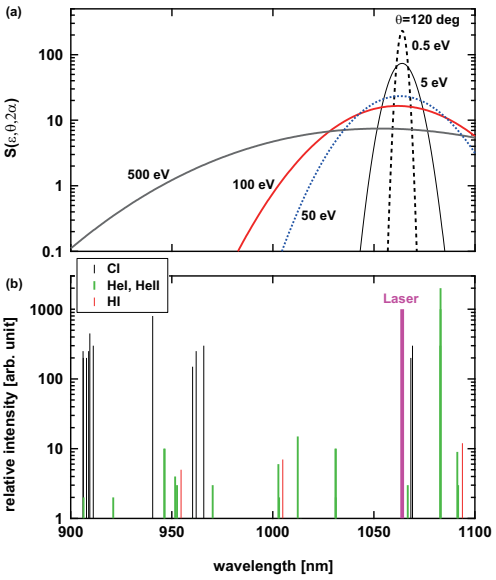

Fig. 3 (a) Spectral density functions at 0.5, 5, 50, 100, and 500 eV for θ_s = 120 degree. (b) relative intensities for impurity lines obtained from NIST database [13].

Optimization of the optical filters used in the polychromator is an important issue for the design study. The optimization is performed by using a developed code, the details of which were described in [12]. For the collection optics, a rhodium coating mirror, four optical lenses and an optical fiber bundle were assumed to be used. The transmissivity of photons is approximately 30%. The noise power is defined as the square root of $N_0 + F_{noise}$×*(photo electrons)*, where N_0 is the dark noise in a time slice, and F_{noise} is the excess noise factor. In the caluculation, N_0 of 30 and F_0 of 2.5 are used in the same manner as in ref. [11]. For the bremsstrahlung intensity, we consider an enhancement factor K_e, which corresponds to the difference between the theoretical and measured bremsstrahlung intensities. The difference may be arisen from the reflection in

Table 2 Major parameters used in the numerical assessment.

Parameter	Value
pulse width	30 [ns]
laser diameter	0.005 [m]
laser pulse energy	5 [J]
laser wavelength	1064 [nm]
length of the scattering volume	0.02 [m]
solid angle	0.005 [str]
scattering angle	120 [degree]
effective path length of the plasma	1.5 [m]
enhancement factor (K_e)	10
excess noise factor (F_{noise})	2.5
dark noise in a time slice (N_0)	30

the vacuum vessel and the emission from impurities. The major parameters required for the calculation were shown in Table 2. In the optimization, the plasma density and temperature for the bremsstrahlung emission are assumed to be 10^{20} m^{-3} and 10 eV, respectively. The density in the measurement region is also assumed to be 10^{20} m^{-3}, while the temperature is changed from 0.5 – 200 eV, which is a little wider range than the required one. In the polychromator, the transmission of optical lens, and the transmission and reflection of optical filter are assumed to be 95%. A collection lens, relay lens, and a optical filter are added as increasing the number of channel. It is also assumed that the optical throughput for the shorter wavelength is better. For the case of $M = 6$, for instance, optical throughputs for the first and sixth channels become 74% and 34%, respectively. The optimized wavelength ranges and measurement performance could be slightly altered when changing the order of the filter channel; however, the effects are not significant and do not influence the following discussion.

Iterative calculation decreases the error in T_e and optimizes the filter segment points. Two different function are used for the optimization. Similar as the previous study, averaged error in T_e, namely,

$$\text{Error} = \overline{\sigma_{T_e}/T_e}, \tag{1}$$

is used for optimization, where σ_{T_e} is the error in T_e, and the averaging is performed by uniformly choosing 50 electron temperatures in the covered temperature range. In addition, following function is also used for optimization in this study:

$$\text{Error} = \sqrt{\left(\overline{\sigma_{T_e}/T_e}\right)^2 + [MAX(\sigma_{T_e}/T_e)]^2}, \tag{2}$$

where $MAX(\sigma_{T_e}/T_e)$ is the maximum value of σ_{T_e}/T_e in the calculated temperature range. Figure 4(a) and (b) show the temperature dependences of σ_{T_e}/T_e optimized with the function of Eq. (1) and Eq. (2), respectively, when the total filter number, M, is 3, 4, and 5. In Fig. 4(a), the error in temperature slightly increases with T_e, and the error is

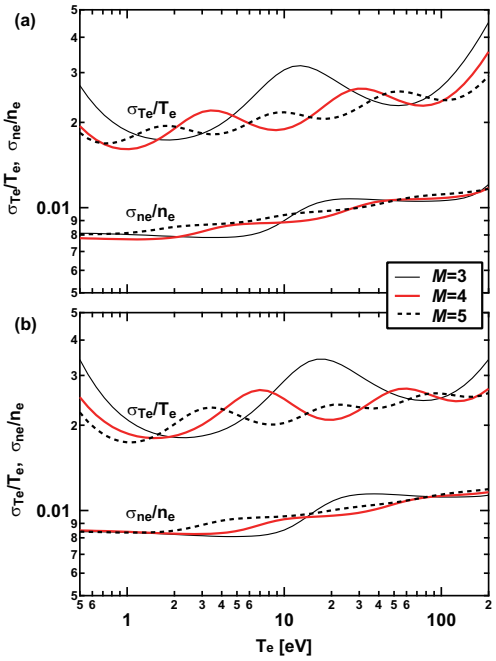

Fig. 4 Temperature dependences of relative error in T_e and n_e for $M = 3$, 4, and 5. Equations (1) and (2) are used in (a) and (b), respectively.

comparatively large when the temperature is high. On the other hand, in Fig. 4(b), the error in the high temperature range is modified because the maximum error is included in the optimization function.

Figure 5(a) and (b) show the averaged and maximum relative errors in T_e, respectively, in the covered temperature range. Optimization was conducted with Eqs. (1) and (2); in each case, two different filter configurations were investigated. In the one case, all the filter segment points are selected from the shorter wavelength than the laser wavelength, while another filter is added above the laser wavelength in the other case. When using Eq. (2) for the optimization, the maximum error significantly decreases, though the averaged error slightly increases, compared to those with using Eq. (1). It is seen that the averaged error has a minimum value at $M = 5$ or 6, while the maximum error decreases with filter number when $M < 4 - 6$, and does not have significant dependence when M is higher. For $M > 5$, it is seen that both errors become smaller when a filter above 1064 nm is used. From the viewpoint of the maximum error, it is shown that a polychromator with four or five detector channels is sufficient.

Figure 6(a) and (b) show the wavelengths of the segment points and the bandwidths of filter, respectively, for $M = 4$, 5, and 6. As the best configuration, the case in which segment points are assigned below 1064 nm is chosen for $M = 4$, and the case in which an filter is assigned above 1064 nm is chosen for $M = 5$ and 6. It is found that the shortest wavelength is approximately 980 nm; thus, the transmission wavelength ranges do not overlap with the

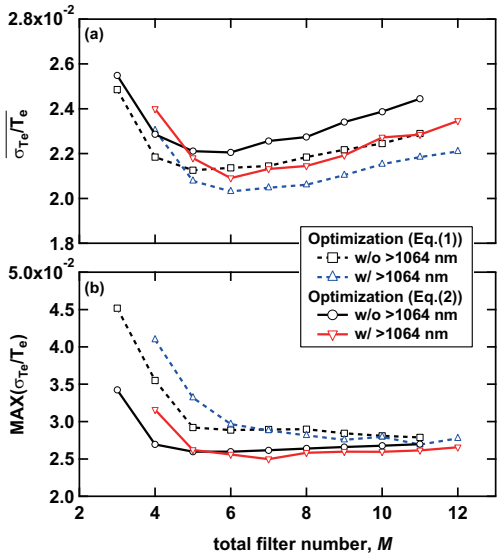

Fig. 5 The total filter number (M) dependences of (a) averaged error in temperature, and (b) maximum error in temperature for different filter configurations.

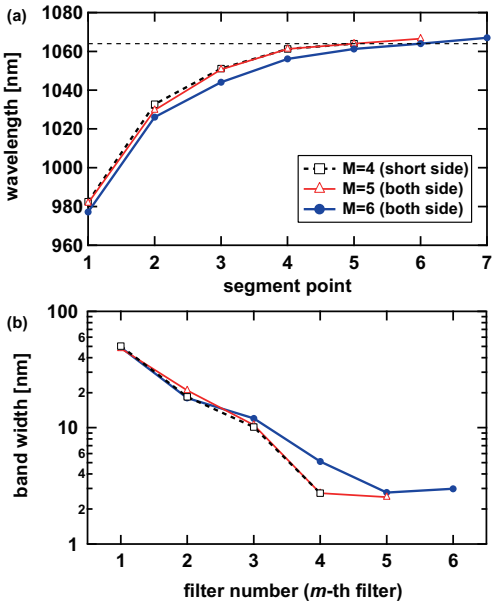

Fig. 6 (a) Optimized wavelengths for segment points and (b) the bandwidths of the filter for M = 4, 5, and 6.

carbon lines shown in Fig. 3(b). The widest bandwidth of the filter is approximately 50 nm, while the narrowest one is approximately 3 nm. Although the calculated segment point above 1064 nm does not overlap with the carbon lines at 1068–1070 nm, the wavelength is so close that it may be hard to reject the impurity lines completely. Moreover, the filter which is adjacent to the laser wavelength is ~ 3 nm, so that there is concern that the optical depth at the laser wavelength should be lower than the expected value of 5–6. Fablication of these optical filters may be crucial for the divertor Thomson scattering system, and the confirmation of the feasiblity remains as a future work.

4 Conclusion

Preliminary design for divertor Thomson scattering measurement system, including first mirror, laser transmission mirror, and detection systems, for JT-60SA is presented. From the view points of the solid angle for collecting scattering signal, laser beam dump to reduce stray light, and damages for laser transmission mirror, it is revealed that both laser transmission optics and collection optical system are to be embedded in the lower port. From the perspective of the laser induced damage threshold, it is thought that cupper mirror is one of good choices; however, it is suggested that laser beam shape should be elliptical to decrease the laser pulse energy at the mirror surface. For the detection system, the performance of the multi-channel polychromator with optical filters is investigated by means of numerical method. To optimize the wavelength ranges of filters, averaged and maximum errors in T_e were combined to be used. The shortest wavelength for optical filters was approximately 980 nm; the calculation revealed that the filter wavelength ranges did not overlap with the impurity lines such as neutral helium and neutral and ionized carbon species. When the filter number was greater than 5, additional filter above 1064 nm would be effective. However, fabrication of the filter adjacent to the laser wavelength may be hard, but a crutial issue, because it should have large optical density at 1064 nm, typically 6, and narrow, typically 3 nm, bandwidth.

For future work, it is necessary to confirm the feasibility of the optical filter with a sufficient optical depth at the laser wavelength. Also, it is important to check that both collection optical system and laser transmission mirror can be embedded in the slender lower port plug.

Acknowledgments

This work was supported in part by a Grant-in-Aid for Young Scientists (B), 21760690, from the Japan Society for the Promotion of Science (JSPS).

[1] N. Ezumi, N. Ohno, K. Aoki, D. Nishijima and S. Takamura, Contrib. Plasma Phys. **38**, S31 (1998).
[2] S. Kajita, S. Kado, N. Ohno, S. Takamura, K. Kurihara and Y. Kuwahara, Phys. Plasmas **14**, 103503 (2007).
[3] S. Kajita, N. Ohno, S. Takamura and T. Nakano, Phys. Plasmas **13**, 013301 (2006); (erratum) **16**, 029901 (2009).
[4] S. Kajita, D. Nishijima, E. M. Hollmann and N. Ohno, Phys. Plasmas **16**, 063303 (2009).
[5] T. N. Carlstrom, C. L. Hsieh, R. Stockdale, D. G. Nilson and D. N. Hill, Rev. Sci. Instrum. **68**, 1195 (1997).
[6] F. Scotti and S. Kado, J. Nucl. Mater. **390-391**, 303 (2009).
[7] S. Kajita, T. Hatae and V. S. Voitsenya, Plasma Fusion Research **3**, 032 (2008).

[8] T. Hatae, O. Naito, M. Nakatsuka and H. Yoshida, Rev. Sci. Instrum. **77**, 10E508 (2006).
[9] J. F. Figueira and S. J. Thomas, IEEE J. Quant. Elec. **QE-18**, 1381 (1982).
[10] T. Hatae, M. Nakatsuka, H. Yoshida, K. Ebisawa, Y. Kusama, K. Sato, A. Katsunuma, H. Kubomura and K. Shinobu, Transactions of Fusion Science and Technology **51**, 58 (2007).
[11] S. Kajita, T. Hatae and Y. Kusama, Rev. Sci. Instrum. **79**, 10E726 (2008).
[12] S. Kajita, T. Hatae and O. Naito, Fusion Engineering and Design **84**, 2214 (2009).
[13] NIST Atomic Spectra Database, url:http://physics.nist.gov/PhysRefData/ASD/index.html.